Received: 3 May 2021 | Revised: 1 June 2021 | Accepted: 10 June 2021

DOI: 10.1049/rsn2.12147

IET Radar, Sonar & Navigation

The Institution of Engineering and Technology WILEY

ORIGINAL RESEARCH PAPER

Time-frequency characterisation of bistatic Doppler signature of a wooded area walk at L-band

Giovanni Manfredi[1] | Israel D. Hinostroza Sáenz[1] | Michel Menelle[2] | Stéphane Saillant[1,2] | Jean-Philippe Ovarlez[1,2] | Laetitia Thirion-Lefevre[1]

[1]SONDRA, CentraleSupélec, Université Paris-Saclay, Gif-sur-Yvette, France

[2]ONERA, Université Paris-Saclay (DEMR/EGDR), Palaiseau, France

Correspondence

Giovanni Manfredi, SONDRA, CentraleSupélec, Université Paris-Saclay, Gif-sur-Yvette 91190, France.
Email: giovanni.manfredi@centralesupelec.fr

Abstract

The Doppler signature of a man walking in a forested area analysed at L-band is presented here. The aim is twofold: to assess the best time-frequency distribution to characterise the activity; to highlight the similarity of the simulated data to the measured ones to validate the simulation tool. Indeed, the Doppler-Time (DT) signal variation represents the main characteristic of Artificial Neural Networks (ANNs) for classification. The more accurately the DT characterises the activity, the higher the machine's accuracy in classifying it. Besides, in the training data frame, reliable simulated models may supply the amount of data needed by ANN applications. Thus, a short-time Fourier transform (STFT), a reassigned spectrogram (RE-Spect), and a pseudo-Wigner–Ville distribution have been applied to the measured and simulated data. The measurements have been performed using a bistatic radar working at 1 GHz. Then, the measurement setup has been replicated in simulation, and 3-D human bodies walking in free space have been computed using physical optics. The results show that the STFT is the most suitable time-frequency method for recognising and classifying the walk. Moreover, the simulated data are in agreement with the measured data, regardless of the chosen Cohen's technique.

1 | INTRODUCTION

Human detection and the activity classification are significant research topics for the surveillance, security, and search-and-rescue operations. The Doppler radar is the widely used technology for the identification and monitoring of human subjects [1, 2]. The main issue for detecting humans is represented by the wide variety of physical activities and positions.

Kim et al. [3, 4] have carried out a classification of different human activities, including running, boxing, walking, crawling, and sitting still. The micro-Doppler signatures have been recorded by a radar working at 2.4 and 7.25 GHz. The classification has been performed by using a support vector machine (SVM) and a deep convolutional neural network (DCNN). Bilik et al. [5] focussed on distinguishing people from animals and wheeled vehicles using new features identification. The targets have been recorded by a 9-GHz ground surveillance pulse-Doppler radar and the corresponding spectrograms have been used for the classification. Park et al. [6] have investigated the micro-Doppler signatures in a more challenging case to classify human activities on water. A DCNN has been implemented to analyse the measured and simulated data collected at 7.25 GHz. Fioranelli et al. have classified the bistatic Doppler signature of indoor human movements [7]. The activities of walking, getting up and sitting from a chair, and picking up an object on the ground have been analysed with a bistatic radar operating at 5.8 GHz (C-band). The impact of different aspect angles on unarmed versus potentially armed personnel classification has been analysed, instead, at 2.4 GHz (S-band) using a multi-static radar [8].

Doppler radars have been also employed to detect human targets in urban centres. The main challenge is to deal with the multipath propagation that may induce the wrong

location of the target [9]. Linnehan et al. have analysed at 16.9 GHz, the Doppler response of a subject moving in urban multipath environments [10]. The Doppler of different walking persons have been analysed by using a radar system behind corners working in continuous wave (CW) at 10 GHz [11, 12].

The analysis of the Doppler response of humans moving within forested areas is an active research topic that has not yet been fully explored. Kilic et al. [13, 14] have presented a study of the effects of the mutual coupling between the forest and a moving subject. A Doppler analysis has been carried out at 5 GHz based entirely on numerical tests. The forest, as well as the human body, have been modelled as being perfectly conductive. Davis has highlighted, with experimental tests, that radars are more efficient operating in L-band (1.3 GHz) and in UHF-band (400 MHz) to detect animals, human subjects, and vehicles moving under heavily wooded regions [15]. However, at these frequencies, the Doppler signature of moving human bodies is expected to be different, as shown by Dogaru et al. using simulated data at 300 MHz in free space [16].

In a previous work [17], we have analysed at L- and UHF-band, the time variation of the frequency signature of a subject walking and running in a wooded area. We have presented the walk and run's measured spectrograms whose backscattering signals have been collected employing a bistatic radar operating at 1 GHz (L-band) and 435 MHz (UHF-band). In this paper, we focus, instead, on the processing of the received signal. Within the Cohen's class, the short-time Fourier transform (STFT) is the most employed function to characterise human activities [2–6, 8, 16]. A time-frequency distribution provides the Doppler-Time (DT) variation of the reflected signal on which machine learning classification is principally based [3, 4, 18–22]. The artificial learning accuracy, therefore, depends on the reliability of the DT feature. In the frame of human sensing in L-band, we wondered which is the best Cohen's class distribution to characterise the DT signature of a walk performed in a forested area. To this purpose, the measured Doppler spectrum has analysed applying the short-time Fourier transform STFT [23], the reassigned spectrogram RE-Spect [24], and the pseudo-Wigner–Ville distribution PWVD [25]. They represent the most used window-based transformation functions to explore the spectrum of a moving subject's time variation. The time-frequency distributions have also been applied to the simulated data representing the backscattered response of a 3-D human body walking in free space. The aim is to evaluate the reliability of the simulated data with respect to the measured ones. The assessment of the time-frequency techniques and simulated data has been performed by analysing four Doppler characteristics extracted from the spectrograms. The simulated and measured features have been compared with those theoretically calculated by implementing different human walking models.

The paper is organised as follows. The bistatic radar system used for the measurements and the numerical tests are described in Section 2. The Doppler frequencies of the walk, theoretically calculated, and the extraction of the Doppler features are analysed in Section 3. The measured and simulated spectrograms relative to the different time-frequency distributions are commented in Section 4. An assessment of the STFT, RE-Spect, and PWVD based on the similarity index between the simulated, measured, and theoretical Doppler features is discussed in Section 5. Finally, the conclusions are presented in Section 6.

2 | BISTATIC RADAR SETUP

The description of the bistatic radar and of the setup chosen for both the numerical tests and the measurements has been presented in the previous work [17]. We summarise the basic parameters as follows.

Two Log periodic antennas have been used working in CW at 1 GHz. The antennas have been mounted at 1.35 m above the ground and located at 0° azimuth and 0° elevation. In addition, the antennas have been positioned at $L = 16$ m apart, so as to ensure a negligible mutual coupling between them. Vertical polarisation has been chosen for the transmitting and receiving antennas.

The measurements have been carried out in an outdoor scene represented by a grass field with the presence of a row of trees, as shown in Figure 1a. The subject has travelled a distance $R = 30$ m in approximately 30 s, walking towards the antennas. In detail, the target started the walk close to the trees at 40 m away from the antennas and he concluded the activity at the distance of 10 m from the radar system, as depicted in Figure 1b. It follows that L and R outline a tracking area characterised by a bistatic angle β, linearly varying from 22.6° to 77.4°.

Two temporal signals have been separately collected: $x_{\text{clutter}(t)}$ denotes the contribution of the clutter to the backscattered field, and $x_{\text{target+clutter}(t)}$ that is the signal reflected by the moving subject in this environment; t refers to the time of the collection. The recorded signals have been first sampled at $f_r = 10$ kHz and the in-phase (I) and the quadrature-phase (Q) components have been extracted. Then, a clutter suppression has been carried out as following:

$$x(t) = x_{target+clutter}(t) - x_{clutter}(t). \tag{1}$$

The subtraction of clutter helps to reduce the impact of the stationary background and antenna coupling. Conversely, it may potentially increase the clutter due to moving branches and leaves [26], albeit at a much lower Doppler shift than that produced by a walking person. Thus, a high pass filter with a cut-off frequency $f_c = 0.1$ Hz has been applied to $x(t)$ to decrease the surrounding environment's impact on the walk's Doppler spectrum.

The measurement setup has been replicated in simulation. A 3-D human model walking at 0.9 m/s has been implemented in MATLAB®, replacing each body part with canonical

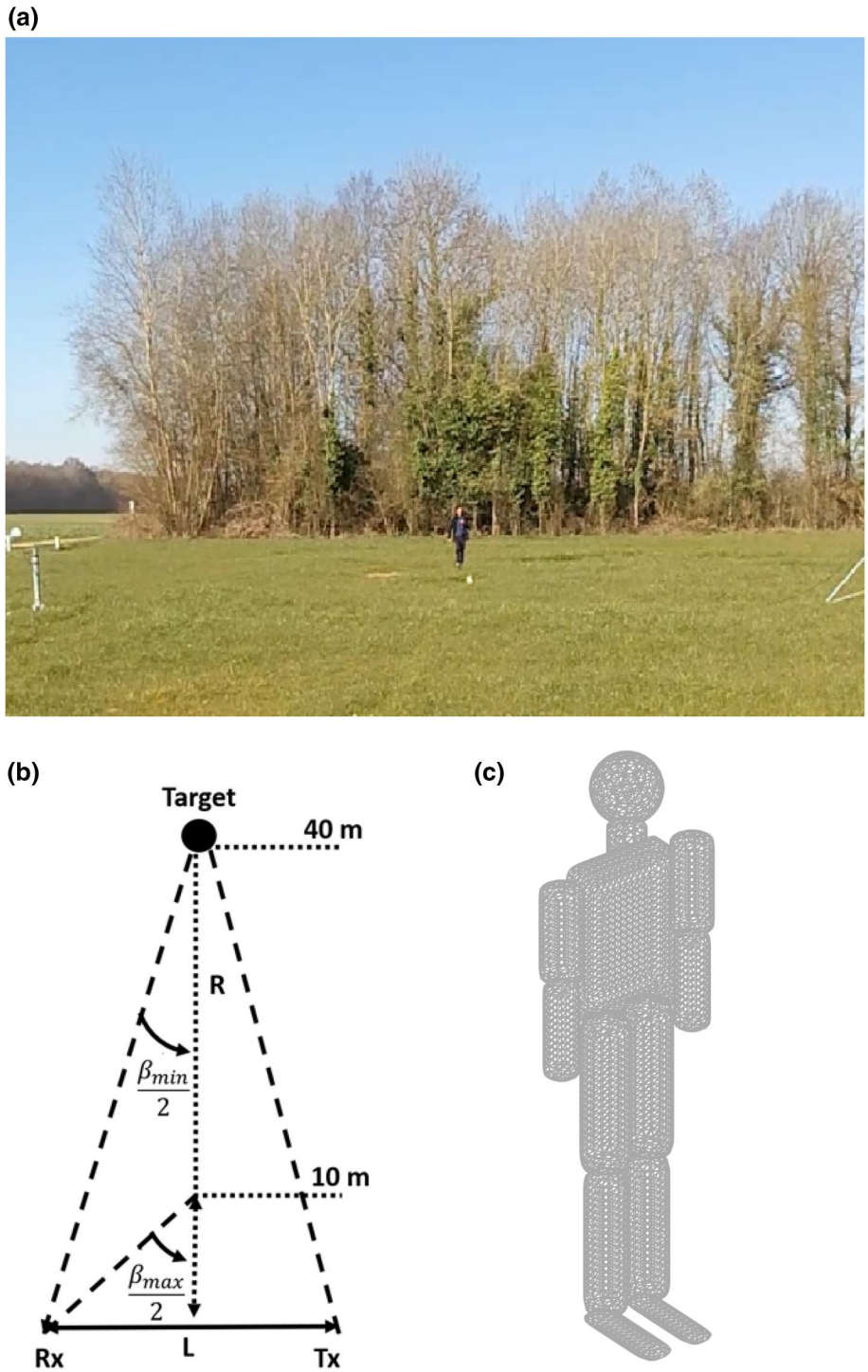

FIGURE 1 Bistatic radar setup: (a) outdoor scene, (b) parameters of the bistatic configuration, (c) 3-D human body model. The subject performed a walk wearing a jacket. The measurements have been carried out in the presence of moderate wind

dielectric shapes (a sphere, cylinders, and a parallelepiped), as represented in Figure 1c. The relative permittivity $\varepsilon_r = 40.94$ and the conductivity $\sigma = 0.9$ S/m have been chosen to simulate the dielectric properties of the dry skin at 1 GHz [27]. The backscattered responses of the moving target have been provided by a simulation tool based on the theory of the physical optics (PO) [28].

3 | CHARACTERISATION OF THE FREQUENCY SIGNATURE OF A WALKING MAN AT 1 GHz

The walk of different moving subjects has been first analysed at 1 GHz theoretically. The Doppler frequencies have been calculated to characterise the physical activity by the

extraction of representative features. To this purpose, four subjects have been simulated, with walking speeds ranging from 0.9 to 1.4 m/s. The motions have been recorded at 120 Hz by the Motion Capture Lab [29]. 3-D human models have been implemented as having 11 body parts to reproduce faithfully the motions of a human walking cycle: right arm (RA), left arm (LA), right forearm (RFA), left forearm (LFA), right thigh (RT), left thigh (LT), right leg (RL) and left leg (LL), head (H), neck (N), and torso (T). Their sizes have been chosen to be equivalent to the average human body sizes [30, 31].

The Doppler frequency modulations have been analytically calculated according to the following equation [32]:

$$F_D = \left(\frac{2\|\vec{v}\|}{\lambda}\right)\cos\left(\frac{\beta}{2}\right), \tag{2}$$

where F_D denotes the Doppler shift, $\vec{v}$ the vector velocity, λ the radar wavelength, and β the bistatic angle. The individual Doppler contributions of the body parts of a subject walking at 0.9 m/s are shown in Figure 2 in an interval time of 4 s, as a representative case. The Doppler frequencies due to the motions of the head, the neck, and the torso are superimposed and less distinguishable from each other. The highest and lowest Doppler shifts are instead caused by the movements of the limbs.

Four features have been chosen to characterise the Doppler signature of the walk [3, 33]: (1) the torso Doppler frequency, (2) the period, (3) the total bandwidth (BW) of the Doppler signal, and (4) the offset. The torso Doppler frequency (1) is related to the speed of the walking man. Period (2) is the time period of the Doppler response from the torso. It corresponds to the half swings rate of the legs. The total BW of the Doppler signal (3) is provided by the highest speed of the upper and the lower limbs. The offset (4) outlines, instead, the asymmetry between the forward and backward motions of the arms and the legs.

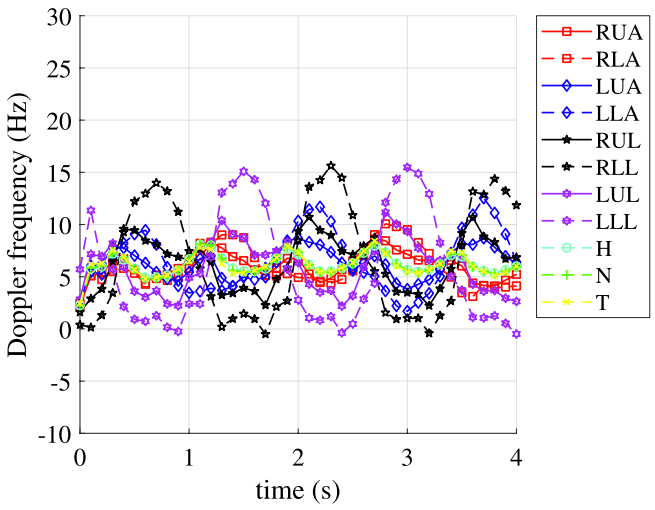

FIGURE 2 Doppler frequencies of a subject walking at 0.9 m/s simulated at 1 GHz

The four features have been automatically extracted by processing the data over each time bin. In the representative case depicted in Figure 2, the torso Doppler frequency (1) is the average frequency of the Doppler contributions provided by the bobbing torso. The result is shown in Figure 3. In the spectra presented in Section 4, the torso Doppler frequency (1) corresponds to the average frequency of the peak signal in intensity processed over each time bin. Then, according to Equation (2), the radial speed is calculated. The period (2) is the time period of the Doppler from the torso shown in Figure 3. The calculation of the features 3) and 4) has been carried out identifying two envelopes [33, 34]: the high-frequency envelope (HFE) and the low-frequency envelope (LFE). Figure 4 shows the two extracted curves by processing

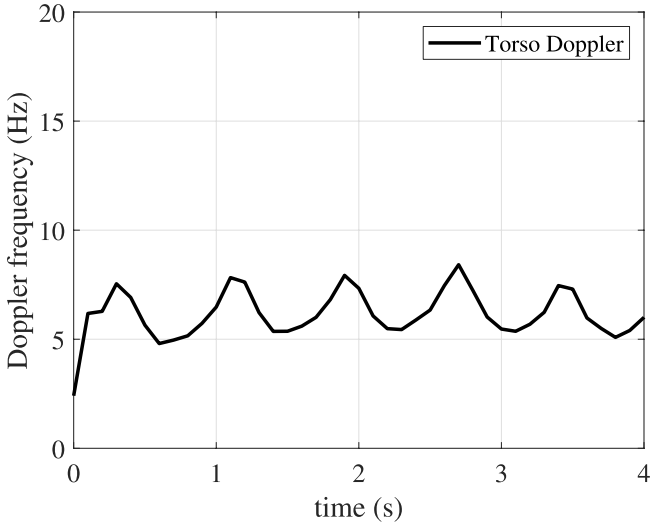

FIGURE 3 Doppler frequencies of the bobbing torso

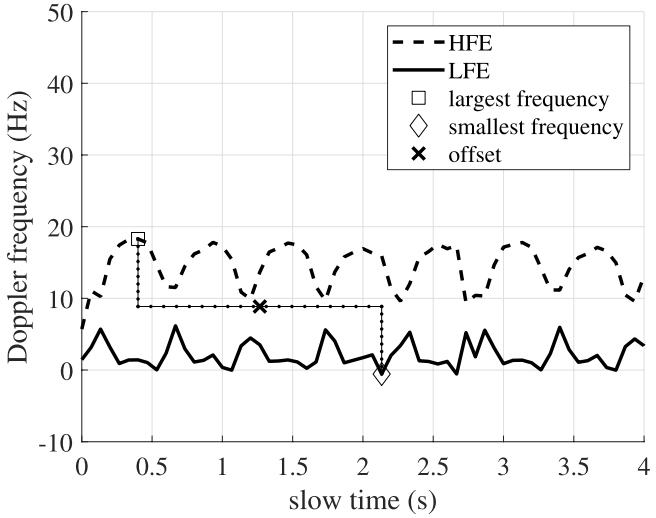

FIGURE 4 Doppler frequency envelopes of a human body model walking at 0.9 m/s: the high-frequency envelope (HFE) (dashed line), the low-frequency envelope (LFE) (continuous line). The square marker represents the largest frequency of HFE, and the diamond marker represents the smallest frequency of LFE. The offset (cross marker) is the mean value between the largest and smallest frequency

the Doppler contributions of a human phantom walking at 0.9 m/s, analysed at 1 GHz. At each time bin, HFE is made up by the highest Doppler frequency, whereas LFE is made up by the lowest Doppler frequency. Thus, the total BW (3) is calculated as the averaged difference between the highest frequency of HFE and the lowest frequency of LFE. The offset (4) is the mean value between the largest frequency of HFE and the smallest of LFE, as shown in Figure 4.

The ranges of values of the Doppler features theoretically calculated are indicated in Table 1. Those characteristics have been used for comparison with those obtained by the simulations and the experimental test. The comparison allows evaluating the best time-frequency analysis for the Doppler characterisation of the walk.

4 | TIME-FREQUENCY DISTRIBUTIONS

The simulated and measured backscattered responses of the walking target have been post-processed by performing an STFT [23], an RE-Spect [35, 36], and a PWVD [37]. The STFT is the widely time-frequency transform used for the identification and classification of different types of human motions [3, 4, 10–13]. The STFT is not characterised by interferences but is known to have very poor joint time-frequency resolutions [38]. The RE-Spect is a technique for refocussing the time-frequency data to achieve high-resolution spectral representations [24]. The PWVD provides more accurate instantaneous frequency and group delay values of the non-stationary multi-component signals [25]. It has moderate performance in terms of joint time-frequency resolution [39]. The three distributions mainly describe the potentiality of performance proposed by the Cohen class.

In a previous work [33], we have highlighted that the choice of a frequency window (Hanning, Hamming, Gauss, Kaiser, and Flattop) does not affect the characterisation of the Doppler signature. Therefore, the Hanning window has been employed within the time-frequency distributions. A coherent processing interval (CPI) equal to 0.5 s has been chosen, which implies a frequency resolution Δf equal to 2 Hz.

The simulated and measured Doppler spectra have been normalised and plotted in dB scale (Figures 5a–7b), where the x-axis represents the slow time, and the y-axis the Doppler frequencies. The normalisation has been carried out to highlight the Doppler frequency distributions of the simulated and measured walk in the same dB range.

TABLE 1 Doppler characteristics of simulated walking subjects, analytically calculated at 1 GHz

Features	1 GHz
(1) Torso Doppler	5.98–9.74 Hz
(2) Period	0.51–0.72 s
(3) Total BW	15.95–32.99 Hz
(4) Offset	7.49–9.8 Hz
Radial speeds	0.9–1.46 m/s

Abbreviation: BW, bandwidth.

4.1 | Short-time Fourier transform

The first analysis focussed on the STFT of the signal backscattered by the target walking towards the antennas. The STFT is defined in continuous time as [23]

$$F_x(t,f) = \int_{-\infty}^{\infty} x(u)\, h^*(u-t)\, e^{-i2\pi f u}\, du, \qquad (3)$$

where $x(.)$ denotes the signal reflected by the moving target, $h(\cdot)$ the smoothing Hanning window, $*$ the complex conjugate, and $S_x(t,f)$ the spectrogram distribution. The so-called spectrogram is defined as the square modulus of the STFT:

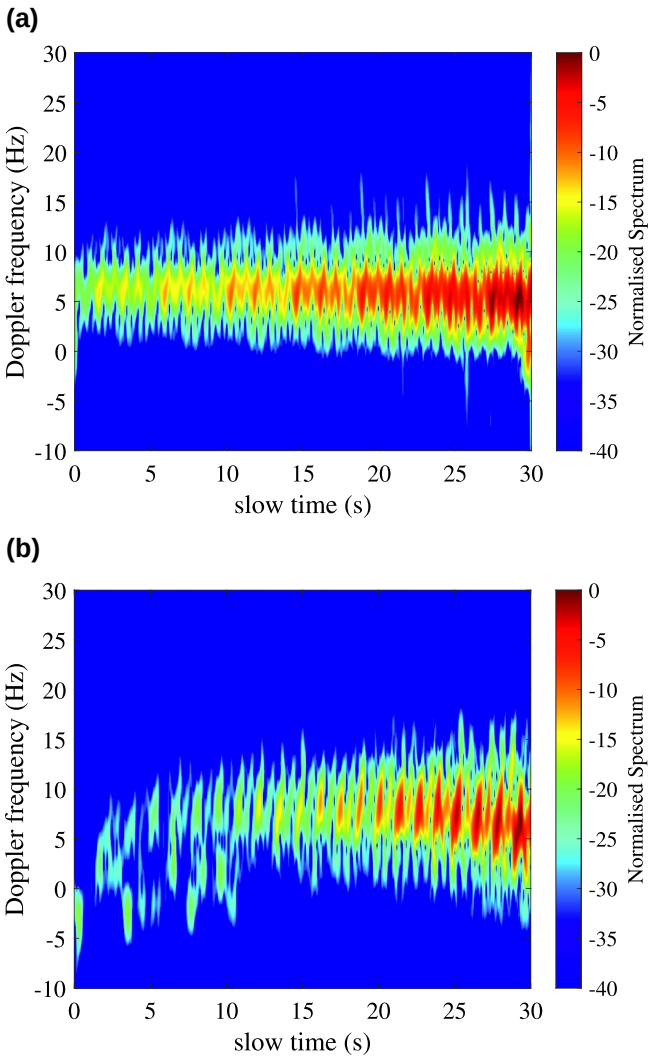

FIGURE 5 Doppler frequency signature of a walking man analysed at 1 GHz by using the short-time Fourier transform: (a) simulated data, (b) measured data

$$S_x(t, f) = |F_x(t, f)|^2. \quad (4)$$

The simulated and measured results are shown in Figure 5a,b, respectively. The corresponding Doppler features are listed in Table 2.

As concerns the simulated signature, the physical activity caused positive Doppler shifts, centred around 6 Hz, meaning a target approaching the antennas. The spectrogram is marked by a high intensity sinusoidal shaped, highlighted by the orange-red pattern depicted in Figure 5a. The pattern is principally related to the swaying torso, head, and neck from which the strongest signal is reflected. It is characterised by the feature (1) equal to 5.97 Hz, which implies a speed equal to 0.9 m/s. The Doppler spectrum appears quite uniform with a period (2) equal to 0.56 s. The cyan spikes observed at the lower and upper edges of the pattern, instead, can be related to the motions of the arms and legs [3, 4]. The speeds of the limbs of the simulated human phantom determine a total BW (3) of 22.53 Hz and their asymmetric movement corresponds to an offset (4) around 6 Hz, as presented in Table 2.

The measured Doppler shifts due to the walking towards the antennas are shown in Figure 5b. The spectrum exhibits a periodic trend which is saw-tooth shaped, well observed starting from 5 s. The detected torso Doppler (1) is 6.25 Hz that corresponds to a speed of 0.94 m/s. The forward motions of the limbs are more detected than those backwards, identified in the positive Doppler pattern by the cyan spikes. Their movement are asymmetric with an offset (4) of 5.1 Hz and characterised by a BW (3) equal to 25.31 Hz. Negative Doppler contributions are also observed in Figure 5b in the first 10 s, highlighted by the green-cyan spikes weak in magnitude. They could be associated to the presence of echoes not related to the main activity. It has to be noted that the measurements have been performed in the presence of moderate wind. Therefore, the slight movements of the undergrowth along with the path, and of the jacket worn by the target, may have caused the observed negative Doppler shifts.

Overall, the measured and simulated features fall within the ranges theoretically calculated (Table 1), except for the offset, as shown in Table 2. The difference may be related to the high variability of asymmetry occurring in the movements of the lower and upper limbs. Indeed, it depends on the performed physical activity, speed, gender and sizes of the subject that are not entirely included in our database. However, the simulated data are in agreement with the measured ones, with differences of around 10%. It is worth noting that the simulation implements a human body walking in free space. Therefore, such differences are considered negligible.

TABLE 2 Short-time Fourier transform: theoretical, simulated, and measured Doppler features of a subject walking near the forest, analysed at 1 GHz

Features	Data	1 GHz
(1) Torso Doppler	theoretical	5.98–9.74 Hz
	simulated	5.97 Hz
	measured	6.25 Hz
(2) Period	theoretical	0.51–0.72 s
	simulated	0.56 s
	measured	0.68 s
(3) Total BW	theoretical	15.95–32.99 Hz
	simulated	22.53 Hz
	measured	25.31 Hz
(4) Offset	theoretical	7.49–9.8 Hz
	simulated	5.96 Hz
	measured	5.1 Hz
Radial speeds	theoretical	0.9–1.46 m/s
	simulated	0.9 m/s
	measured	0.94 m/s

4.2 | Reassigned spectrogram

The simulated and measured data have been further analysed by using the RE-Spect. This technique enhances the resolution both in the time and in the frequency domain, making the spectrogram less blurred around the single instantaneous frequencies [40]. The RE-Spect [35, 41] is acting on Equation (4) according to

$$S_x^{(r)}(t', f') = \int_{-\infty}^{+\infty}\int_{-\infty}^{+\infty} S_x(t,f)\,\delta\left(t' - \hat{t}(x;t,f)\right) \delta\left(f' - \hat{f}(x;t,f)\right) dt\,df, \quad (5)$$

where the new corresponding centres of energy $\hat{t}(x;t,f)$ in time and $\hat{f}(x;t,f)$ in frequency are given by the following:

$$\hat{t}(x;t,f) = t + \mathrm{Re}\left\{\frac{F_x(t,f;T_h)}{F_x(t,f;h)}\right\}, \quad (6)$$

$$\hat{f}(x;t,f) = f - \mathrm{Im}\left\{\frac{F_x(t,f;D_h)}{F_x(t,f;h)}\right\}, \quad (7)$$

with $F_x(t,f)$ defined in Equation (3) and where $T_h(t) = t\,h(t)$ and $D_h(t) = dh(t)/dt$ represent, respectively, the operators of multiplication and differentiation, where δ is the Dirac delta function and $\mathrm{Re}\{\cdot\}$, $\mathrm{Im}\{\cdot\}$ stand for the real and imaginary parts, respectively, of the resulting complex number.

The simulated and measured results are shown in Figure 6a,b, respectively. The time-frequency plots look sharper than those observed in Figure 5a,b. The simulated and measured Doppler patterns of the main reflective area of the moving body characterised by the features (1) are equal to 5.96 and 5.63 Hz, as presented in Table 3. They denote radial speeds equal to 0.89 and 0.84 m/s,

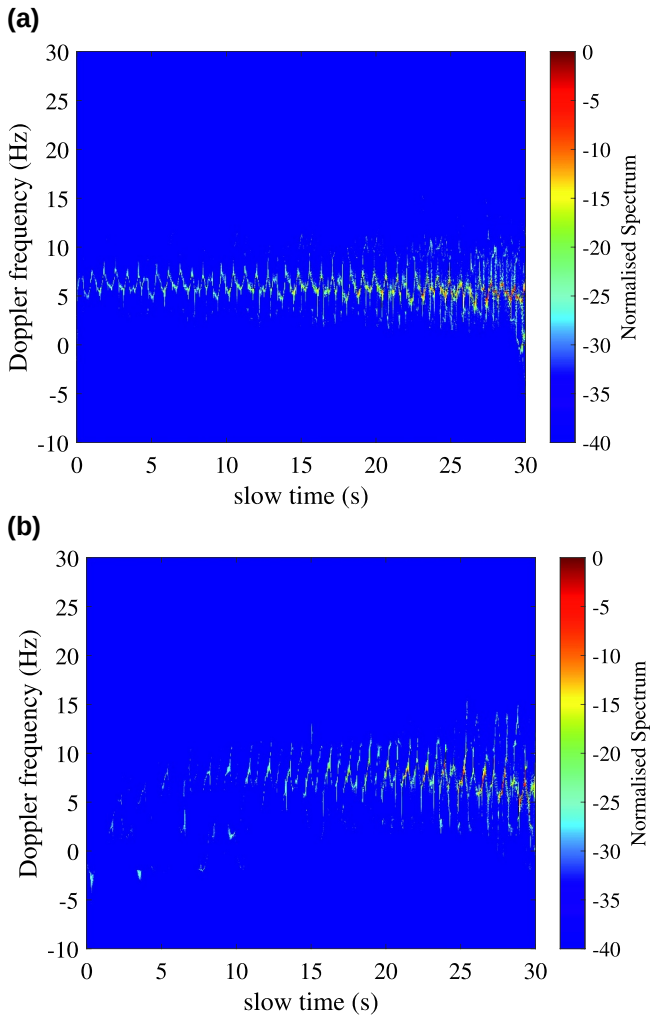

FIGURE 6 Doppler frequency signature of a walking man analysed at 1 GHz by using the RE-Spect: (a) simulated data, (b) measured data

respectively, nearly in agreement with the theoretical ones. The Doppler pattern looks periodic and saw-tooth shaped with period (2) equal to 0.71 and 0.67 s, relative to the simulated and measured frequency signatures.

The Doppler shifts due to the limb motions are difficult to detect and observable only in the time interval 20–30 s. Consequently, the routine process makes a mistake, evaluating a Doppler BW (3) smaller than those observed in Table 2, applying the STFT, and an offset (4) outside the theoretical range presented in Table 1. An explanation is that the Doppler contributions due to the movement of the body parts are less separated and distinguishable from each other, due to the low chosen working frequency. Unfortunately, one of the main constraints in the reassignment-based technique is the separability condition on the individual signal components. The Doppler frequencies are correctly reassigned to their corresponding mode, as long as the criteria for separability are fulfilled [42, 43].

Therefore, the RE-Spect method proves not to be suitable faithfully for the characterisation and classification of the walk at 1 GHz.

TABLE 3 Reassignment spectrogram: theoretical, simulated, and measured Doppler features of a subject walking near the forest, analysed at 1 GHz

Features	Data	1 GHz
(1) Torso Doppler	theoretical	5.98–9.74 Hz
	simulated	5.96 Hz
	measured	5.63 Hz
(2) Period	theoretical	0.51–0.72 s
	simulated	0.71 s
	measured	0.67 s
(3) Total BW	theoretical	15.95–32.99 Hz
	simulated	18.19 Hz
	measured	21.15 Hz
4) Offset	theoretical	7.49–9.8 Hz
	simulated	6.49 Hz
	measured	5.1 Hz
Radial speeds	theoretical	0.9–1.46 m/s
	simulated	0.89 m/s
	measured	0.84 m/s

4.3 | Pseudo-Wigner–Ville distribution

At last, the PWVD has been applied to the simulated and measured backscattered data. The distribution is given by the following expression [25, 44]:

$$PWVD_x(t,f) = \int_{-\infty}^{+\infty} h(\tau)\, K_x(t,\tau)\, e^{-i2\pi f\tau}\, d\tau, \qquad (8)$$

where $K_x(t, \tau)$ is the kernel function of the Wigner–Ville distribution defined as

$$K_x(t,\tau) = x(t-\tau/2)\, x^*(t+\tau/2). \qquad (9)$$

The spectrograms are shown in Figure 7 and the corresponding features listed in Table 4. The PWVD, as well as the RE-Spect, allows to accurately detect the instantaneous frequency and group delay values characterising the observed walk. The torso Doppler feature (1) of around 5.9 Hz implies a simulated and measured speed equal to 0.89 m/s, thus, in perfect agreement with each other. Moreover, the radial speeds of the Table 4, as well as the simulated and measured period (2), are in accordance with the corresponding ranges theoretically calculated and listed in Table 1.

Reversely, the Doppler contributions due to the forward and backward motions of the arms and legs are strongly blurred by unwanted frequency components, represented by the cyan bands shown in Figure 7a,b. Indeed, due to the bilinearity transform of the PWVD, the Doppler spectra are affected by interference terms, especially when the frequencies

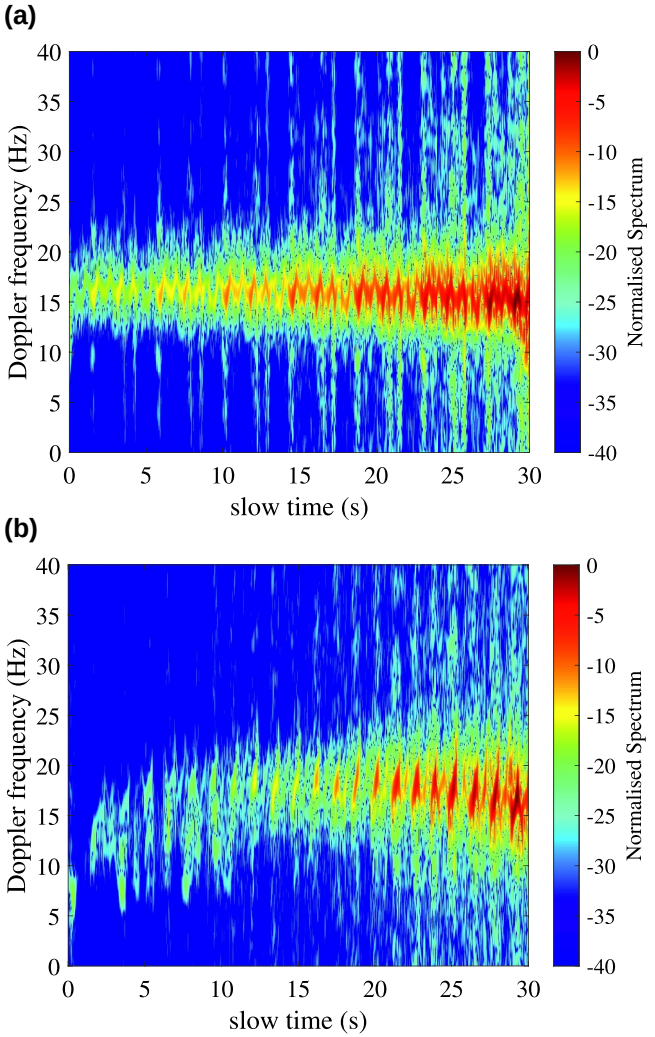

FIGURE 7 Doppler frequency signature of a walking man analysed at 1 GHz by using the pseudo-Wigner–Ville distribution: (a) simulated data, (b) measured data

TABLE 4 Pseudo-Wigner–Vile distribution: theoretical, simulated, and measured Doppler features of a subject walking near the forest, analysed at 1 GHz

Features	Data	1 GHz
(1) Torso Doppler	theoretical	5.98–9.74 Hz
	simulated	5.97 Hz
	measured	5.95 Hz
(2) Period	theoretical	0.51–0.72 s
	simulated	0.72 s
	measured	0.66 s
(3) Total BW	theoretical	15.95–32.99 Hz
	simulated	60 Hz
	measured	60 Hz
(4) Offset	theoretical	7.49–9.8 Hz
	simulated	20 Hz
	measured	20 Hz
Radial speeds	theoretical	0.9–1.46 m/s
	simulated	0.89 m/s
	measured	0.89 m/s

TABLE 5 Rating based on the similarity index i_s

i_s range values	Rating
(0.95, 1)	★ ★ ★ ★ ★
(0.8, 0.95)	★ ★ ★ ★
(0.65, 0.8)	★ ★ ★
(0.5, 0.65)	★ ★
(<0.5)	★

swiftly change [45]. As a result, the BW (3) and the offset (4) equal to 60 and 20 Hz prove to be unreasonable and do not allow to correctly identify the walk.

5 | DISCUSSIONS

A final evaluation of the used Doppler techniques is summarised in this section. For this purpose, a ratio between the data presented in Table 1 and those listed in Tables 2–4 was performed for each Doppler characteristic and radial speed. Thus, the similarity index i_s (value between 0 and 1) of the measured and simulated data with respect to the theoretical ones is calculated. The final result is represented through stars as shown in Table 5. The index i_s allows discriminating the best window-based transformation function to characterise the walk's frequency signature at 1 GHz through its Doppler features. Furthermore, it highlights the simulated data's conformity with the measured ones.

The period, torso Doppler, and, consequently, the walk's radial speed are well identified independently of the performed joint time-frequency analysis, as shown in the Table A1, although RE-Spect provides a lower similarity index than STFT and PWVD. However, these features are not sufficient to characterise physical activity. The Doppler bandwidth and the offset allow distinguishing walks performed at different speeds or other activities such as running, boxing, and crawling [17, 34]. In this respect, PWVD provides unreasonable values that do not allow the observed physical activity's correct characterisation. Better values of offset and Doppler bandwidth are obtained by applying an STFT and an RE-Spect instead. Offset continues to be the most critical parameter to detect from a spectrogram. Nevertheless, we believe that the differences between the simulated and measured data with those theoretically calculated are due to a database that is still not sufficiently robust. It does not incorporate the enormous variability of asymmetries that a walk can originate based on the gender, size, and speed under examination. Further walking models must therefore be integrated into the database.

Overall, the STFT is the Doppler technique that best classifies the walk at 1 GHz. The low time-frequency resolution did not influence the correctness of the data, as shown in Table 2 comparing the experimental and simulated data with the theoretical ones, and highlighted by the i_s values of each feature listed in Table A1.

Finally, it is worth noting that the simulated data are always in almost complete agreement with the experimental data, regardless of the used technique. The simulations have been performed by faithfully reproducing the experimental setup but without modelling the surrounding environment. The 3-D human body models move in free space. The simulated spectrograms are in perfect agreement with the measured ones regarding the received signal strength, Doppler signature periodicity, mean Doppler frequency, and Doppler band dynamics. These are distinctive features of the spectrum of physical activity. The only difference is the initial shape of the spectrum, characterised by an acceleration of the target, which is not considered in the simulation. This difference is not relevant in the detection, characterisation, and classification of the observed activity as demonstrated by the conformity of the simulated data with those measured in Tables 2–4. The simulation tool proves to be sufficiently accurate for our purposes. At low frequency, the characterisation and classification of physical activities carried out in forest areas could be performed through machine learning in future work. Therefore, the availability of valid models for human scattering can overcome the problem of the amount of needed data that cannot be supplied by measurements alone.

6 | CONCLUSIONS

In this paper, the assessment of the best window-based transformation function to identify the Doppler spectrum of a man walking in a forested area at 1 GHz has been presented. To this purpose, the STFT, the RE-Spect, and the PWVD have been applied to the simulated and measured data. Besides, four Doppler features have been extracted from the spectra to characterise the physical activity. The RE-Spect and the PWVD provide accurate Torso Doppler frequency, and consequently, they allow the detection of the radial speed assumed by the moving target accurately. On the other hand, either the Doppler shifts caused by the asymmetric limb motions are not easily detectable with the RE-Spect, or the cross-terms of the PWVD blur them. Conversely, the STFT correctly provides the Doppler characteristics of the physical activity, proving suitable for the characterisation and classification at 1 GHz of a walk performed in an outdoor scene.

ACKNOWLEDGEMENTS

The author wishes to thank the Carnegie Mellon University – CMU Graphics Lab.

ORCID

Giovanni Manfredi https://orcid.org/0000-0002-2857-7886

REFERENCES

1. Vandersmissen, B., et al.: Indoor person identification using a low-power FMCW radar. IEEE Trans. Geosci. Rem. Sens, 56(7), 3941–3952 (2018)
2. Vignaud, L., et al.: Radar high resolution range & micro-Doppler analysis of human motions. In: 2009 International Radar Conference "Surveillance for a Safer World" (RADAR 2009), pp. 1–6. IEEE (2009)
3. Kim, Y., Ling, H.: Human activity classification based on micro-Doppler signatures using a support vector machine. IEEE Trans. Geosci. Rem. Sens. 47.(5), 1328–1337 (2009)
4. Kim, Y., Moon, T.: Human detection and activity classification based on micro-Doppler signatures using deep convolutional neural networks. Geosci. Rem. Sens. Lett. IEEE. 13(1), 8–12 (2016)
5. Bilik, I., Tabrikian, J., Cohen, A.: GMM-based target classification for ground surveillance Doppler radar IEEE Trans. Aero. Electron Syst. 42(1), 267–278 (2006)
6. Park, J., et al.: Micro-Doppler based classification of human aquatic activities via transfer learning of convolutional neural networks. Sensors. 16(12), 1990 (2016)
7. Fioranelli, F., Ritchie, M., Griffiths, H.: Bistatic human micro-Doppler signatures for classification of indoor activities. In: 2017 IEEE Radar Conference (RadarConf), pp. 0610–0615. IEEE (2017)
8. Fioranelli, F., Ritchie, M., Griffiths, H.: Performance analysis of centroid and SVD features for personnel recognition using multistatic micro-Doppler. Geosci. Rem. Sens. Lett. IEEE. 13(5), 725–729 (2016)
9. Setlur, P., Amin, M., Ahmad, F.: Multipath model and exploitation in through-the-wall and urban radar sensing. IEEE Trans. Geosci. Rem. Sens. 49(10), 4021–4034 (2011)
10. Linnehan, R., Schindler, J.: Multistatic scattering from moving targets in multipath environments. In: 2009 IEEE Radar Conference, pp. 1–6. IEEE (2009)
11. Sume, A., et al.: Radar detection of moving targets behind corners. IEEE Trans. Geosci. Rem. Sens. 49(6), 2259–2267 (2011)
12. Gustafsson, M., et al.: Extraction of human micro-Doppler signature in an urban environment using a "sensing-behind-the-corner" radar. Geosci. Rem. Sens. Lett. IEEE. 13(2), 187–191 (2016)
13. Kilic, O., et al.: Detection of moving human micro-Doppler signature in forest environments with swaying tree components by wind. Radio Sci. 50(3), 238–248 (2015)
14. Garcia Rubia, J.M., et al.: Analysis of moving human micro-Doppler signature in forest environments. Progr. Electromagn. Res. 148, 1–14 (2014)
15. Davis, M.E.: FOPEN radar design for sparse forest surveillance. In: 2016 IEEE Radar Conference (RadarConf), pp. 1–6. IEEE (2016)
16. Dogaru, T., Le, C., Kirose, G.: Time-Frequency Analysis of a Moving Human Doppler Signature. U.S. Army Research Laboratory (2009)
17. Manfredi, G., et al.: Measurements and analysis of the Doppler signature of a human moving within the forest in UHF-band. Rem. Sens. 13(3), 423 (2021)
18. Javier, R.J., Kim, Y.: Application of linear predictive coding for human activity classification based on micro-Doppler signatures. Geosci. Rem. Sens. Lett. IEEE. 11(10), 1831–1834 (2014)
19. Alnujaim, I., Oh, D., Kim, Y.: Generative adversarial networks to augment micro-Doppler signatures for the classification of human activity. In: IGARSS 2019 – 2019 IEEE International Geoscience and Remote Sensing Symposium, pp. 9459–9461. IEEE (2019)
20. Ye, W., Chen, H.: Human activity classification based on micro-Doppler signatures by multiscale and multitask Fourier convolutional neural network. IEEE Sensor J. 20(10), 5473–5479 (2020)
21. Dong, S., et al.: Radar-based human identification using deep neural network for long-term stability. IET Radar Sonar Navig. 14(10), 1521–1527 (2020)
22. Ni, Z., Huang, B.: Human identification based on natural gait micro-Doppler signatures using deep transfer learning. IET Radar Sonar Navig. 14(10), 1640–1646 (2020)
23. Chen, V.C., Qian, S.: Joint time-frequency transform for radar range-Doppler imaging. IEEE Trans. Aero. Electron. Syst. 34(2), 486–499 (1998)

24. Hansson Sandsten, M., Brynolfsson, J.: The scaled reassigned spectrogram with perfect localization for estimation of Gaussian functions. IEEE Signal Proc. Lett. 22(1), 100–104 (2015)
25. Xu, Z., Carrion, L., Maciejko, R.: An assessment of the Wigner distribution method in Doppler OCT. Opt. Express. 15(22), 14738 (2007)
26. Sizov, V., et al.: Vegetation clutter spectral properties in VHF/UHF bistatic Doppler radar. In: 2008 IEEE Radar Conference, pp. 1–6. IEEE (2008)
27. Istituto di Fisica Applicata Nello Carrara: Dielectric Properties of Body Tissues. http://niremf.ifac.cnr.it/tissprop/htmlclie/htmlclie.php. Accessed 29 April 2021
28. Manfredi, G., et al.: Efficient simulation tool to characterize the radar cross section of a pedestrian in near field. Progr. Electromagn. Res. C. 100, 145–159 (2020)
29. Carnegie Mellon University: CMU Graphics Lab Motion Capture Database. mocap.cs.cmu.edu. Accessed 29 April 2021
30. Schwind, A., Stephan, R., Thuringian, M.A.H.: Simulations and measurements of the bistatic radar cross section of vulnerable road users between 2 GHz and 6 GHz. In: 2018 IEEE MTT-S International Conference on Microwaves for Intelligent Mobility (ICMIM), pp. 1–4. IEEE (2018)
31. Poston, A.: Human Engineering Design Data Digest: Human Factors Standardization Systems. Human Factors Standardization SubTAG (2000)
32. Willis, N.J.: Bistatic Radar. Institution of Engineering and Technology (2004)
33. Manfredi, G., Ovarlez, J.P., Thirion Lefevre, L.: Features extraction of the Doppler frequency signature of a human walking at 1 GHz. In: IGARSS 2019 – 2019 IEEE International Geoscience and Remote Sensing Symposium, pp. 2260–2263. IEEE (2019)
34. Kim, Y., Ling, H.: Human activity classification based on micro-Doppler signatures using a support vector machine. IEEE Trans Geosci. Rem. Sens. 47(5), 1328–1337 (2009)
35. Auger, F., Flandrin, P.: Improving the readability of time-frequency and time-scale representations by the reassignment method. IEEE Trans. Signal Proc. 43(5), 1068–1089 (1995)
36. Reinhold, I., Starkhammar, J., Sandsten, M.: The scaled reassigned spectrogram adapted for detection and localisation of transient signals. In: 2017 25th European Signal Processing Conference (EUSIPCO), pp. 907–911. IEEE (2017)
37. Tan, R., et al.: Improved micro-Doppler features extraction using Smoothed-Pseudo Wigner-Ville Distribution. In: 2016 IEEE Region 10 Conference (TENCON), pp. 730–733. IEEE (2016)
38. Chen, V.C., Qian, S.: Joint time-frequency transform for radar range-Doppler imaging. IEEE Trans. Aero. Electron. Syst. 34(2), 486–499 (1998)
39. Boashash, B., Ouelha, S.: Designing high-resolution time–frequency and time–scale distributions for the analysis and classification of non-stationary signals: a tutorial review with a comparison of features performance. Digit. Signal Proc. 77, 120–152 (2018)
40. Bruni, V., Tartaglione, M., Vitulano, D.: On the time-frequency reassignment of interfering modes in multicomponent FM signals. In: 2018 26th European Signal Processing Conference (EUSIPCO), pp. 722–726. IEEE (2018)
41. Flandrin, P., Auger, F., Chassande Mottin, E.: Time-frequency reassignment: from principles to algorithms. In: Papandreou-Suppappola, A., Applications in Time-Frequency Signal Processing, pp. 179–204. CRC Press (2018). https://www.taylorfrancis.com/chapters/edit/10.1201/9781315220017-5/time-frequency-reassignment-principles-algorithms-flandrin-auger-chassande-mottin
42. Meignen, S., Oberlin, T., Wu, H.T.: Selective time-frequency reassignment based on synchrosqueezing. IEEE Signal Proc. Lett. 22(11), 2039–2043 (2015)
43. Fitz, K.R., Fulop, S.A.: A unified theory of time-frequency reassignment. arXiv Preprint. arXiv:09033080 (2009)
44. Ren, H., Ren, A., Li, Z.: A new strategy for the suppression of cross-terms in pseudo Wigner–Ville distribution. Signal Image Video Proc. 10(1), 139–144 (2014)
45. Fan, L., Evans, D.H.: Extracting instantaneous mean frequency information from Doppler signals using the Wigner distribution function. Ultrasound Med. Biol. 20(5), 429–443 (1994)

How to cite this article: Manfredi, G., et al.: Time-frequency characterisation of bistatic Doppler signature of a wooded area walk at L-band. IET Radar Sonar Navig. 15(12), 1573–1582 (2021). https://doi.org/10.1049/rsn2.12147

APPENDIX A

Table A1 shows the rating of the STFT, RE-Spect, and PWVD applied to the simulated and measured data.

TABLE A1 Assessment of the STFT, RE-Spect, and PWVD, through the analysis of the index i_s between the simulated/measured Doppler features and the theoretical ones

	STFT		RE-Spect		PWVD	
Doppler features	**Simulated**	**Measured**	**Simulated**	**Measured**	**Simulated**	**Measured**
(1) Torso Doppler	★ ★ ★ ★	★ ★ ★ ★	★ ★ ★ ★	★ ★ ★	★ ★ ★ ★	★ ★ ★ ★
(2) Period	★ ★ ★ ★	★ ★ ★ ★	★ ★ ★ ★	★ ★ ★ ★	★ ★ ★ ★	★ ★ ★ ★
(3) Total BW	★ ★ ★	★ ★ ★	★ ★ ★	★ ★ ★	★	★
(4) Offset	★ ★ ★	★ ★	★ ★ ★	★ ★	★	★
Radial speed	★ ★ ★ ★	★ ★ ★ ★	★ ★ ★ ★	★ ★ ★	★ ★ ★ ★	★ ★ ★ ★

Abbreviations: BW, bandwidth; PWVD, pseudo-Wigner–Ville distribution; RE-Spect, reassigned spectrogram; STFT, short-time Fourier transform.